Journal of Power Sources 227 (2013) 161–170

Contents lists available at SciVerse ScienceDirect

Journal of Power Sources

journal homepage: www.elsevier.com/locate/jpowsour

Model-based simultaneous optimization of multiple design parameters for lithium-ion batteries for maximization of energy density

Sumitava De, Paul W.C. Northrop, Venkatasailanathan Ramadesigan, Venkat R. Subramanian*

Department of Energy, Environmental and Chemical Engineering, Washington University, St. Louis, MO 63130, USA

HIGHLIGHTS

- ► Optimization of electrode design parameters for maximization of energy density.
- ► Model-based simultaneous optimization of design parameters.
- ► Increased computational efficiency provided by reformulated model.

ARTICLE INFO

Article history:
Received 16 August 2012
Received in revised form
26 October 2012
Accepted 13 November 2012
Available online 20 November 2012

Keywords:
Lithium-ion batteries
Model-based design
Optimization
Physics based reformulated model

ABSTRACT

A model-based procedure is applied to the simultaneous optimization of design parameters for porous electrodes that are commonly used in advanced batteries such as lithium-ion systems. The approach simultaneously optimizes the battery design variables of electrode porosities and thickness for maximization of the energy drawn for an applied current, cut-off voltage, and total time of discharge. The results show reasonable improvement in the specific energy drawn from the lithium-ion battery when the design parameters are simultaneously optimized. Model simulation and multi-parameter optimization were facilitated by the increased computational efficiency achieved from the use of an orthogonal collocation-based reformulated model.

1. Introduction

Electrochemical power sources have been identified as major players in sectors like automobiles, power storage, military, and space applications. Lithium-ion batteries, in particular, have a wide range of applications ranging from low power/low energy applications such as implantable cardiovascular defibrillators (ICDs) to high power/high energy applications such as hybrid cars and power grids. This paper considers the simultaneous optimization of battery design parameters such as the thickness of the electrodes and porosity of the materials to maximize the specific energy of the battery to meet the needs of future applications.

Although mathematical modeling of lithium-ion batteries is still considered challenging, major contributions have been made in this field. Doyle et al. [1] developed a first-principles model based on concentrated solution theory for a lithium-ion sandwich consisting of a porous electrode, separator, and current collectors. This is the most widely used physics-based model in the battery literature giving accurate predictions even for high rates of charge and discharge and has been used previously for optimization purposes [2–5].

Models for lithium-ion batteries were further developed [6–17], with several literature reviews available [14–17]. Transport phenomena models are most suitable for the design of batteries due to their ability to provide accurate predictions of the internal and external behavior at the system level. These models are based on porous electrode theory coupled with transport phenomena and electrochemical reaction engineering [1,6–14,18]. One consideration in battery optimization is the computational cost of simulating these types of battery models. Circuit-based empirical battery models are convenient due to their low computational costs but have the tendency to fail at many operating conditions and can produce inaccurate predictions [19]. These considerations have motivated the application of model reduction methods to porous electrode theory models. Proper orthogonal decomposition has been applied to the full numerical solution of a lithium-ion battery model to fit a reduced set of eigenvalues and nodes to obtain a lower order approximate solution [20]. An alternative approach is

* Corresponding author. Tel.: +1 314 935 5676; fax: +1 314 935 7211.
E-mail address: vsubramanian@seas.wustl.edu (V.R. Subramanian).

0378-7753/$ – see front matter © 2012 Elsevier B.V. All rights reserved.
http://dx.doi.org/10.1016/j.jpowsour.2012.11.035

model reformulation of lithium-ion battery porous electrode theory models to increase the computational efficiency without losing accuracy. Previously, Subramanian et al. [21] reformulated the widely used isothermal pseudo-2D porous electrode model for galvanostatic boundary conditions. That model provided an approach for simulating battery models in milliseconds without sacrificing accuracy, but had difficulties when nonlinear properties and thermal effects were considered. Northrop et al. [22] presented a coordinate transformation method combined with an orthogonal collocation-based reformulation for the simulation of lithium-ion battery operation. This reformulation [22] is designed to be computationally efficient while maintaining the fidelity of the porous electrode theory model even for high rates of charge and discharge. Forman et al. [23] developed a reduced order electrochemistry based battery model which has sufficient speed and fidelity to enable design, optimization and control. Newman and others have reported methods to obtain optimal values of design parameters such as electrode thickness [2–5,24,25]. Newman [24] describes the use of a reaction zone model for fast electrode kinetics to optimize for electrode thickness and porosity. Although these studies have the advantage of having analytical solutions, they have some limitations and do not include all the physics of the original models. Newman and his co-workers report the use of Ragone plots for studies on the optimization of battery design parameters [2–5]. By changing one design parameter, such as the electrode thickness, at a time and keeping other parameters constant, Ragone plots for different configurations can be obtained. Hundreds of simulations are required when the applied current is varied to generate a single curve in a Ragone plot, which is tedious and has many computational constraints. Previous work by Ramadesigan et al. [25] optimized the porosity distribution by minimizing ohmic resistance of a porous electrode, as a proof of concept.

Golmon et al. [26] attempted a multiscale design optimization for improving electrochemical and mechanical performance of the battery by manipulating both micro- and macro-scale design variables such as local porosities, particle radii and electrode thickness to minimize internal stresses and maximize the capacity of the battery. A surrogate-based framework using global sensitivity analysis has been used to optimize electrode properties [27].

To our knowledge, simultaneous optimization of multiple battery design parameters using first-principles physics-based models have not been reported in the literature due to high computational expense coupled with the need to perform numerous simulations during the optimization. The objective of this study is to simultaneously optimize battery design parameters (i.e., electrode thickness, porosity of active materials) to maximize the specific energy obtained from the battery. A robust optimization routine is implemented that employs the reformulated model developed by Northrop et al. [22] in order to take advantage of its computational efficiency. The continuous need for improving the performance of electrochemical power sources motivates the investigation of robust optimization of battery design and operating conditions.

2. Optimization and design considerations

The integral of the instantaneous power delivered over the time of discharge of the battery gives the specific energy E in J kg^{-1} [2]

$$E = \frac{1}{M}\int_0^{t_d} V i_{app}\,dt \tag{1}$$

which is dependent on the applied current (input) and potential (output) which changes with time. Simulations were run ranging from 0.1 C to 6 C (relative to the base parameters) for a discharge cut-off potential of 2.8 V and the values of E were calculated and maximized. The mass per unit area of cell M in units of kg m^{-2} is defined by the following equation [2]

$$\begin{aligned} M = {} & \rho_p l_p\left(1-\varepsilon_p-\varepsilon_{f,p}\right)+\rho_n l_n\left(1-\varepsilon_n-\varepsilon_{f,n}\right) \\ & +\rho_e\left(l_p\varepsilon_p+l_s+l_n\varepsilon_n\right)+\rho_f\left(l_p\varepsilon_{f,p}+l_n\varepsilon_{f,n}\right) \end{aligned} \tag{2}$$

which includes composite electrodes and separator, but not current collectors or residual masses. As M is a function of the electrode thicknesses l_p and l_n and porosities ε_p and ε_n, specific energy depends on these design parameters. There is a scope for optimization of these design parameters to maximize the specific energy drawn from the battery for a desired value of applied current and cut-off potential (in other words, for a specific application). Particle radius, although an important design parameter, was neglected here. If this model was used for optimization of particle radius, it would have predicted the smallest particle radius to minimize diffusion limitations across the particle. Other problems related to small particle size exist like increased solvent reduction and oxidation, particularly on the first cycle and difficulty in achieving current efficiency of more than 0.9999 for 5000 deep discharge cycles. As our model is not designed to capture these phenomena, the exclusion of particle size from the optimized parameters list can be justified. Generally, electrolyte is added in excess as it just acts as an excess source for Li ions and a conducting medium for the ions from one electrode to other, hence, electrolyte concentration may not be a design variable. When optimization tests were run, it was found that for any concentration >0.5 M, there was no significant limitation arising from concentration limitations. However, this can change for a different cell, chemistry or electrolyte. The cross-sectional area of the cell could be included as an additional optimization parameter and would likely provide very interesting results. However, for simplicity we decided to limit our analysis to thickness and porosity of the electrodes. Optimization of width was beyond the scope, and the height and width of electrodes are kept constant. This is done to keep the number of optimized variables manageable.

A general formulation for the optimization of a system is

$$\begin{aligned} & \min_{\mathbf{z}(x),\mathbf{u}(x),\mathbf{p}} \boldsymbol{\Phi} \\ & s.t.\frac{dz}{dx} = f\left(\mathbf{z}(x),\mathbf{y}(x),\mathbf{u}(x),\mathbf{p}\right), \quad f\left(z(0)\right) = 0, \\ & \quad g\left(z(1)\right) = 0 \; g(\mathbf{z}(x),\mathbf{y}(x),\mathbf{u}(x),\mathbf{p}) = 0, \; u_L \le \mathbf{u}(x) \le u_U, \\ & \quad y_L \le \mathbf{y}(x) \le y_U, \quad z_L \le \mathbf{z}(x) \le z_U \end{aligned} \tag{3}$$

where $\boldsymbol{\Phi}$ is the dependent variable being optimized, $\mathbf{z}(x)$ is the vector of differential state variables, $\mathbf{y}(x)$ is the vector of algebraic variables, $\mathbf{u}(x)$ is the vector of control variables, and $\mathbf{p}$ is the vector of parameters. The control vector parameterization (CVP) [28] is a widely applied method employed in this study, due to its ease of implementation. This parameterization approximates the infinite-dimensional optimal control problem (3) by a finite-dimensional optimization. Different optimization formulations are possible depending on how the gradient of the resulting nonlinear program is calculated; the computational efficiency of CVP can be increased by incorporating parameter sensitivities. While there have been advances in recent years in the field of dynamic and global optimization [29], these algorithms are still too computationally expensive to be used for applications such as electrochemical systems, which are usually highly stiff in nature with highly

nonlinear kinetics requiring adaptive time-stepping, stiff solvers, etc. It is not expected that the simultaneous simulation-optimization approach [28], which fixes the time or independent variable discretization *a priori* will be computationally efficient for most lithium-ion battery applications.

The adopted procedure employs an efficient mathematical reformulation of the pseudo-2D battery model [21,22] that is much more computationally efficient than using a full-order finite-difference model and is a viable candidate to be used for the optimization of electrode design parameters. This model ignores stress and capacity fade mechanisms. It neglects micro-structural effects and the pseudo continuum model is assumed to be valid for the range of design parameters.

The model simulation with base parameters was performed for the specified cut-off voltage to obtain the base discharge time, which was later used to implement a time constraint in the optimization procedure. Numerical algorithms for optimization can get stuck in local optima, which can be nontrivial to trouble-shoot when the number of optimization parameters is large. This problem can at least be partly addressed using a sequential step-by-step approach. The steps below show the procedure of advancing from one-parameter to four-parameter optimization by using the optimized results from previous step as the initial conditions in the next step which facilitate rapid convergence and achievement of global maxima. The model was simulated with the optimized parameters to compare the electrochemical behavior with the base case. This entire optimization protocol is shown graphically in Fig. 1, and can be summarized in the following steps:

1. Choose a battery model that can predict the optimization objective and is sensitive to the manipulated variables (e.g., a P2D model)
2. Develop a reformulation or reduce the order of the model for efficient simulation. This model should be valid in the range of manipulated variables for optimization.
3. Simulate model obtained in step (2) with the base parameters to obtain the time constraint for optimization.
4. Maximize specific energy by optimizing the first chosen parameter i.e. l_p providing the base parameter value as the initial guess.
5. Simulate model obtained in step (2) with the optimized parameter to check whether the time constraint is satisfied or not and to compare the electrochemical performance with the base parameters.
6. Using the solution from step (4) for l_p and base value for porosity ε_p, as the initial guesses maximize specific energy by optimizing the two parameters simultaneously.
7. Repeat step (5) with the optimized parameters.
8. Add the other variables to be optimized one by one following steps similar to (6) and (7) and finally reach optimal performance with multiple optimized parameters.

Although not described in detail in many textbooks, such approaches that optimize the most sensitive parameters first and then move on to less sensitive parameters are commonly applied in practice as a way to accelerate convergence. Our objective for using this procedure, however, was different. We were interested in knowing whether the potential benefits of optimizing the thickness of a positive electrode would be limited if the porosities were fixed. The model was simulated with the optimized parameters to compare the electrochemical behavior with the base case. The parameters were optimized within respective bounds to ensure against model failure due to prediction of physically unacceptable optimized parameter values. Note that battery models often fail due to difficulties finding consistent initial conditions, which were handled by using robust initialization procedures described elsewhere [30]. The model is likely to break down for very small particle radius or very large particle radius, poor conductivity of solid-phase material, and other extreme situations, but validity of the continuum model is the beyond the scope of this paper. Simulation was performed with the

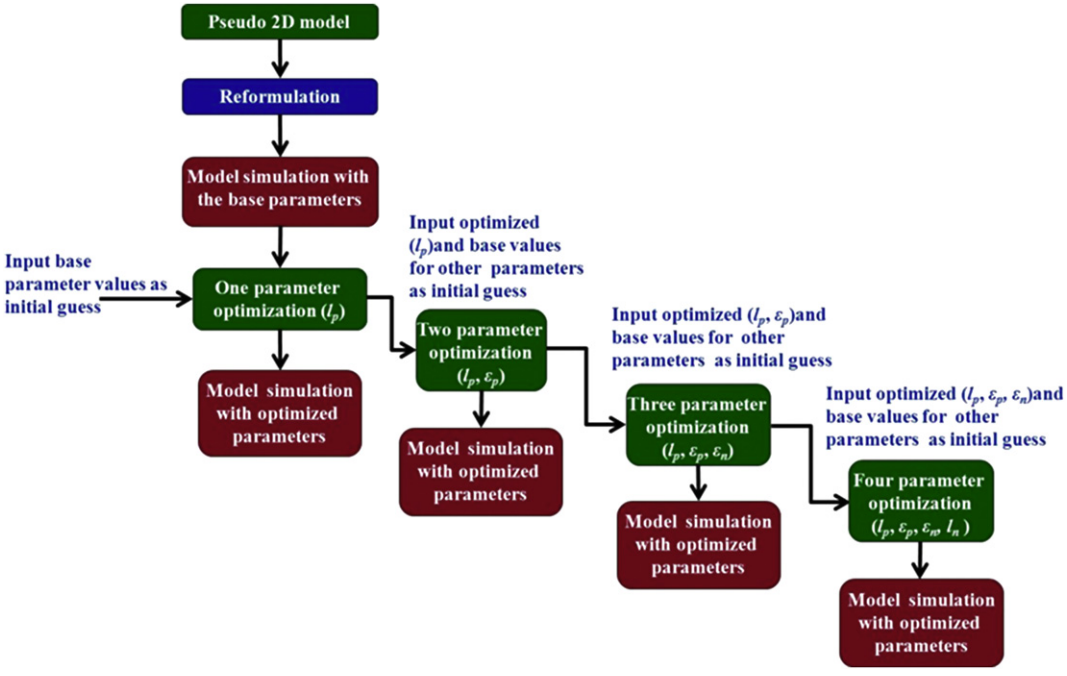

Fig. 1. Steps for evaluation of the importance of and simultaneous optimization of electrode design variables.

reformulated model [22] using the *dsolve* solver in Maple®, multivariable optimization with Maple's *globalsolve* function (Global Optimization Toolbox), and *fmincon* in Matlab®. The protocol in Fig. 1 consistently converged to the same optima found using the more computationally expensive software platforms. The optimization involved optimizing for a fixed rate (say 2 C) with the nonlinear constraint so that the performance was not compromised at lower rates (1 C).

Simulations were first run for different values of applied current and a specific cut-off potential with the base parameters for the thickness and porosities of electrodes to determine the total discharge time t_{d0} for the battery. The applied currents were varied from 0.1 C to 6 C rates. The value for a 1 C rate was found using the applied current for which the total time of discharge was 1 h for the base parameters. Table 1 shows the applied discharge currents for which optimization was performed as well as the total discharge time for each rate. The obtained energy decreases gradually with increase in i_{app}, the applied current density, which is expected because mass transport and kinetic limitations increase the internal resistance of the cell. Fig. 2 presents the variation of specific energy with changing i_{app} when simulated using the base parameters listed in Table 2. The optimization of the electrode design parameters was performed in such a manner that the total discharge time t_d determined from simulation with the optimized parameters was not less than 99% of the original discharge time obtained with the base parameters (i.e. $0.99t_{d0} \leq t_d \leq t_{d0}$) for a specific applied current and fixed cut-off potential of 2.8 V. If this nonlinear constraint is not specified, a higher total energy density could be obtained but the battery may not last long enough for a given application (i.e. for a specific cycle, the battery will get depleted at a shorter time which is not useful for the application).

3. Results and discussions

3.1. One-parameter optimization

The first optimized design parameter was the thickness of the positive electrode (i.e. cathode). Although the thickness of the positive electrode, l_p, was directly optimized, the ratio of the thicknesses of electrodes was fixed as $l_n/l_p = 1.1$ to ensure that the battery was cathode-limited. The cathode to anode thickness ratio was kept fixed but the anode thickness varied according to it for the optimization protocol. Lower and upper bounds for l_p were set as 40 and 90 microns. The aim can be stated as: maximize the energy density, E, such that the partial differential equations governing the battery model are satisfied with optimized parameter values within their respective bounds along with the constrained conditions for l_n, while ensuring that the battery lasts for a specified minimum duration for a given rate of discharge. Mathematically, this can be represented as follows:

$$\max\ E(l_p) = \frac{1}{M}\int_0^{t_d} Vi_{app}\,dt$$

subject to the constraints

$$\begin{aligned} &\frac{dy}{dt} = f(y,u) \\ &g(y,u) = 0 \\ &40\ \mu m \leq l_p \leq 90\ \mu m \\ &0.99t_{d0} \leq t_d \leq t_{d0} \\ &l_n = 1.1l_p \end{aligned} \tag{4}$$

where the differential and algebraic equations were derived from the partial differential equations for the battery model.

Fig. 3 compares specific energy densities drawn from the battery for the 1-parameter optimization vs. the base case, which are very similar due to the tight constraint on the discharge time. As mentioned earlier, an increase in applied current density results in a decrease in the specific energy for both the base parameters and one-parameter optimization cases but no considerable improvement is observed for the optimized case from the base case. Any reduction in the electrode thickness will reduce the mass per unit area of the cell, but also reduces the capacity, ensuring that the battery does not meet the minimum discharge time requirements, while increasing the thickness results in increasing the capacity but results in underutilization. This limits our ability to optimize l_p for the battery with strict discharge time constraint to give optimized parameters which make physical sense. Due to this reason, the

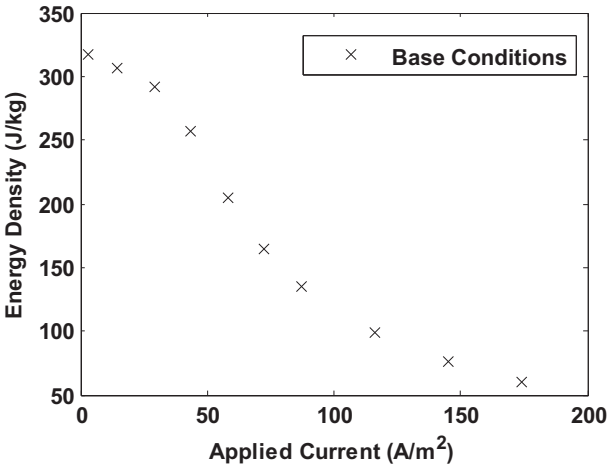

Fig. 2. Plot of the energy density drawn from the battery vs. the applied current for the base case.

Table 1
Applied discharge currents and total discharge times.

Applied current density (A m^{-2})	Discharge time t_{d0} (s)
2.89875	36,478
14.49375	7274
28.9875	3600
43.48125	2189
57.975	1318
72.46875	852
86.9625	592
115.95	329
144.9375	204
173.925	136

Table 2
Base battery design parameters.

Definition of parameters	Base values
Thickness of cathode (l_p)	80 μm
Thickness of anode (l_n)	88 μm
Porosity of cathode (ε_p)	0.385
Porosity of anode (ε_n)	0.485

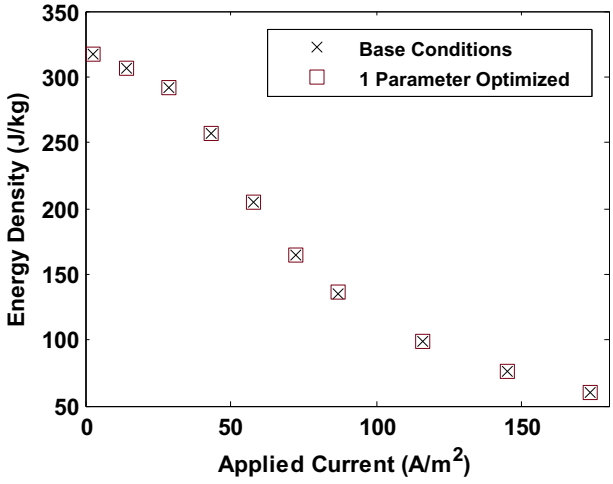

Fig. 3. Plot of the energy density drawn from the battery vs. the applied current for the base case and the one-parameter optimization.

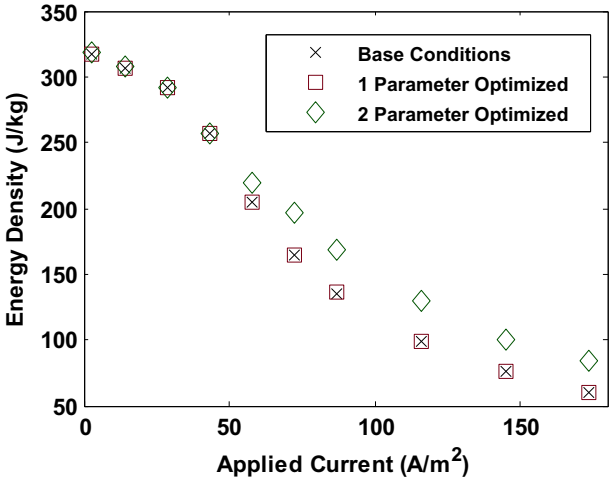

Fig. 4. Plot of energy density drawn from the battery vs. applied current for the two-parameter optimization. The base case is plotted for comparison with the optimized cases.

specific energy obtained from the cell with optimized cathode thickness does not increase much compared to those from the base parameters. The optimal electrode thickness would be different from the base case if the discharge time constraint was relaxed and a considerable improvement in the specific energy drawn from the cell would be observed. This result shows simultaneous optimization of two or more parameters is necessary if an increase in energy drawn is desired without loss in capacity and fulfilling discharge time requirements for specific applications.

3.2. Two-parameter optimization

Here the thickness (l_p) and porosity (ε_p) of the cathode were the design parameters optimized to maximize the energy density. The optimization was again performed by considering a fixed electrode thickness ratio of 1.1. Lower and upper bounds for ε_p were maintained at 0.29 to 0.5, respectively, while the bounds for l_p were retained as in the previous case. The optimization statement is given below.

$$\begin{aligned}
&\max\ E(l_p, \varepsilon_p) = \frac{1}{M}\int_0^{t_d} Vi_{app}\,dt \\
&\text{subject to the constraints} \\
&\frac{dy}{dt} = f(y,u) \\
&g(y,u) = 0 \\
&[40\ \mu m, 0.29]^T \le [l_p, \varepsilon_p]^T \le [90\ \mu m, 0.5]^T \\
&0.99t_{d0} \le t_d \le t_{d0} \\
&l_n = 1.1 l_p
\end{aligned} \tag{5}$$

Fig. 4 compares the specific energy profiles for this case with the one-parameter optimized and base parameter cases. The strict constraint for minimum discharge time was maintained during the optimization protocol. A significant improvement in the specific energy was obtained compared to both the base and one-parameter optimization cases thus proving the importance of simultaneous optimization of design parameters. The improvement is not considerable for lower current densities but is significant for the higher values of current density. Quantitatively, there is almost a 25% increase in energy density compared to the base case for an applied current density, i_{app}, of 86.9625 A m^{-2}. The enhanced performance compared to the base case for some values of i_{app} is due to improved behavior of the internal variables which will be discussed in the later sections. For operation at higher current densities, more transport limitations are faced compared to lower currents. Therefore, optimization of cathode design parameters, improves the performance of the kinetic and transport variables which in turn provides the enhanced performance of the cell by increasing the energy drawn significantly. By inspection of the optimal (l_p, ε_p) for each value of the applied current, it was observed that allowing the porosity to be adjusted freed the electrode thickness to be adjusted much more significantly while satisfying the constraints. The behavior of the optimized parameters will be discussed in detail in the coming sections. Nevertheless, this study proved the importance of simultaneous design parameter optimization for improvement of cell behavior.

3.3. Three-parameter optimization

The parameters optimized were the electrode thickness, porosity of the cathode, and porosity of the anode (ε_n). The upper and lower bounds on the porosity of the anode were 0.36 and 0.61, respectively. The bounds for the cathode parameters were identical to those mentioned for the previously discussed cases. The constraint for minimum discharge time requirements is still valid for the scheme. The optimization protocol is given below.

$$\begin{aligned}
&\max\ E(l_p, \varepsilon_p, \varepsilon_n) = \frac{1}{M}\int_0^{t_d} Vi_{app}\,dt \\
&\frac{dy}{dt} = f(y,u) \\
&g(y,u) = 0 \\
&[40\ \mu m, 0.29, 0.36]^T \le [l_p, \varepsilon_p, \varepsilon_n]^T \le [90\ \mu m, 0.5, 0.61]^T \\
&0.99t_{d0} \le t_d \le t_{d0} \\
&l_n = 1.1 l_p
\end{aligned} \tag{6}$$

Fig. 5 compares the specific energy drawn from the cell for the 3-parameter optimization case with the previously discussed

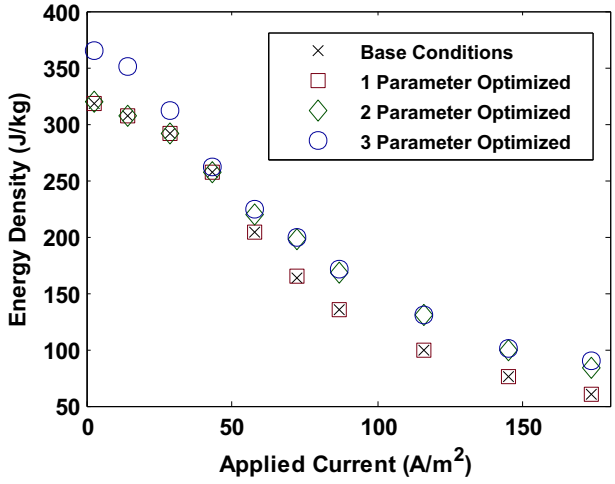

Fig. 5. Plot of the energy density drawn from the battery vs. applied current for the three-parameter optimization. The base case is plotted for comparison with the optimized cases.

optimization protocols and base parameters. Three-parameter optimization achieved higher specific energy compared to one-parameter optimization and base parameter cases, but for low values of the applied current density, the 3-parameter optimization results have much higher energy density than the 2-parameter optimization (see Fig. 5). For high values of applied current density (e.g., for $i_{app} = 86.9625$ A m^{-2} and beyond), optimization of the anode porosity provided a small increase in energy density over optimization of the cathode porosity and cathode thickness. This is because the parameters were optimized with the discharge time constraint which does not allow them to go beyond a certain limit. As soon as the anode porosity was made to be an optimized parameter within specified physically acceptable bounds, it allowed the cathode porosity and cathode thickness to be adjusted accordingly to give high specific energy, especially at the low current density cases while still maintaining the conditions for discharge time constraint. This is because it lowers the porosities for the electrodes which enhances the kinetic and transport behavior at low rates rather than high rates which are discussed in detail later. These results also tell us that at all applied current densities 3-parameter optimization is not necessary to get the best performance from the cell. As shown here, optimization of cathode parameters are enough to get more specific energy for high current densities. This analysis is true for the chemistry chosen, and might vary for other chemistry or designs.

3.4. Four parameter optimization

In this case all the four electrode design parameters (thickness and porosity for both the electrodes) were selected for optimization simultaneously. For this optimization protocol, the anode thickness was optimized just like the other parameters, with upper and lower bounds of 32 microns and 108 microns respectively. The electrode thickness ratio of 1.1 maintained for each of the previously discussed optimization schemes was therefore neglected. The strict discharge time constraint was still applied to the protocol. Previously the optimization protocols always maintained that the anode thickness was always greater than the cathode thickness. This case was simulated to allow the anode thickness to drop below the cathode thickness. The other parameters retained the same upper and lower bounds as in the previous routines. The above mentioned protocol can be expressed mathematically as following:

$$\begin{aligned}
&\max E(l_p, \varepsilon_p, \varepsilon_n, l_n)\\
&\frac{dy}{dt} = f(y,u)\\
&g(y,u) = 0\\
&y = \text{set of differential state variables}\\
&u = \text{set of algebraic variables}\\
&E = \frac{1}{M}\int_0^{t_d} V i_{app} dt\\
&[40\ \mu m, 0.29, 0.36, 32\ \mu m]^T \le [l_p, \varepsilon_p, \varepsilon_n, l_n]^T\\
&\le [90\ \mu m, 0.5, 0.61, 108\ \mu m]^T\\
&0.99 t_{d0} \le t_d \le t_{d0}
\end{aligned} \tag{7}$$

It should be noted that the four parameter estimation is shown only for demonstration purposes. Typically, lithium-ion batteries are manufactured such that the anode capacity is greater than cathode capacity, due to cost. Moreover, the maintenance of the cathode to anode thickness is necessary to match the capacities on both positive and negative sides of the cell. For this reason, the fixed ratio of the electrode thicknesses used for the other optimization cases is considered more meaningful for real world applications. Fig. 6 is intended to show the comparison of energy drawn for four parameter optimization compared to all the other previously mentioned cases of simulation. As expected four parameters optimized simultaneously is the best option from the point of view of maximization of energy, but not practically relevant because of the relatively inexpensive anode materials compared to cathode materials. Examining the plot, it is visible that for higher applied current values the results from four parameter optimization case show significant improvement compared to 3-parameter optimization case. Previously it was seen that the 3-parameter optimization did not improve the drawn specific energy compared to the 2-parameter optimization case at higher values of applied current. As mentioned earlier these results are just for demonstration purposes and they may not be of practical significance as the anode

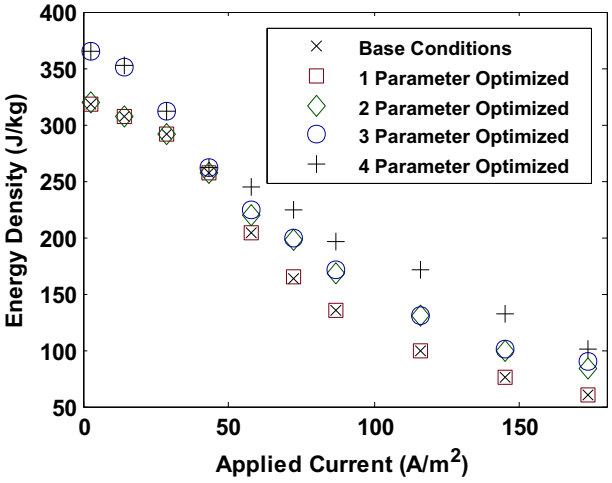

Fig. 6. Plot of specific energy drawn from the battery vs applied current for four parameter optimization. The base case was plotted for comparison with the optimized cases.

thickness was optimized simultaneously with the other variables without maintaining the electrode thickness constraint.

3.5. Electrochemical behavior

One of the main advantages of using physics-based models is the ability to understand the physical behavior associated with an optimal battery design. Empirical models are often valid only across a small range of scenarios. When empirical models are used for optimization, they usually converge to meaningless solutions and the internal non-measurable variables cannot be analyzed. The design parameters from the results from empirical model-based optimization may not make sense when given as input and simulated with physics-based models. The below simulations were performed with the optimized parameters obtained from all the cases for all the values of discharge current.

3.6. Internal behavior

Simulations performed with the optimized parameters for all cases show improved electrochemical and transport behavior, which increases the specific energy. We compare the electrochemical behavior at higher rates (e.g. 2C rate) as improved performance is more visible at high rates. Fig. 7a shows the surface solid-phase concentration at the interfaces for a 2 C rate of discharge. In all cases, the capacity in the electrodes is nearly fully utilized in the region near the separator, as indicated by the rapid increase (for the cathode) and decrease (in the anode) of the surface concentration at the beginning of discharge which tapers off near the end (□ & ◇). However, less capacity is used near the current collectors for all cases (○ & Δ) due to the mass transfer resistance of the porous electrodes. The optimization minimized this resistance and allowed a greater portion of the electrodes to be utilized, as shown in the solid line of Fig. 7a. It is clear from the plots that there is an enhancement in the utilization of the active material in the electrodes to improve performance with the simultaneous optimization of multiple design parameters. For 1-parameter optimization there is no significant performance enhancement but the 3-parameter optimization clearly improves the utilization marked with improved cell performance and increased specific energy. Fig. 7b shows the variation of electrolyte concentration within the cell at different regions, the cathode, the separator and the anode during discharge for different optimization scenarios for 2C discharge rate. We see that the electrolyte concentration for the two-parameter optimization is closer to the equilibrium (initial) concentration of 1000 mol m^{-3} compared to the other cases. If the specific system cannot withstand or handle a high drain in the liquid phase or very low electrolyte concentrations in the anode region, the two-parameter optimization results should be used ignoring the three-parameter optimization results. On the other hand, if the system can withstand the magnitude of starvation of electrolyte, the three-parameter optimization results can be used to get the maximum energy density. Thus, based on variations of the intrinsic variables, we can decide on the number of design parameters to be optimized or the type of results that we can use for that specific system. This is not possible when doing a trial and error based design, or model-based design based on empirical models, and is one of the advantages of using a physics-based model for optimal design.

3.7. Optimized parameters

Variation of the optimized parameters vs. applied current density for all of the optimization protocols were plotted and compared with the base values, which is represented as a straight

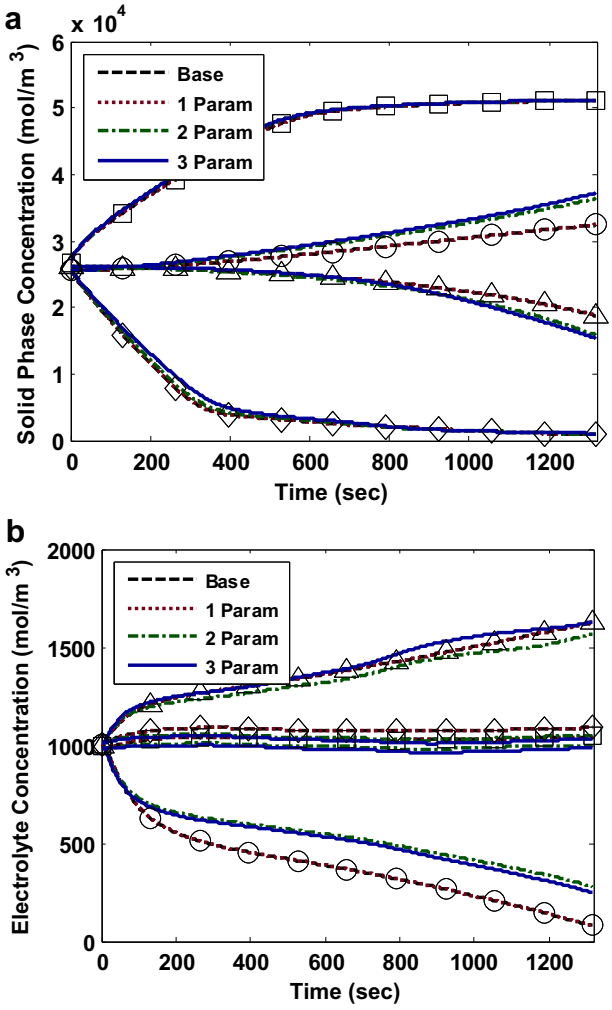

Fig. 7. a. Solid-phase surface concentration throughout discharge for a 2 C rate. b. Electrolyte concentration throughout discharge for a 2 C rate. The (○) is at the current collector cathode interface, (□) for the cathode separator interface, (◇) for the separator-anode interface, and (△) for the anode-current collector interface.

line in the plots given in Figs. 8–11. Fig. 8 shows the variation of optimal cathode thickness for specified applied current densities, while Figs. 9 and 10 show the optimal cathode and anode porosity variations. Fig. 11 represents the optimal anode thickness l_n variation for specified applied current densities which is only valid for 4-parameter optimization case. Data for optimized values for cathode thickness l_p is available for all four cases of optimization while cathode porosity can be plotted only for 2, 3 and 4-parameter optimization cases and anode porosity for 3 and 4-parameter optimization cases only. In general, but not always, applications with higher discharge rates require higher porosities and smaller electrode thicknesses. This design reduces mass transfer resistances within the cell, which can be a limiting factor at higher rates. At low discharge rates, the cell capacity is limiting, so lower porosities and greater thicknesses are preferred. The strict discharge time constraint in the optimization protocol helps control all the factors affecting the kinetic and transport behavior of the cell correctly so as to obtain optimized design parameters which are suitable for specific applications and make physical sense. Looking at the variation of the optimized cathode thickness, for 1-parameter optimization there is not much change in optimized values compared with the base values which is reflected in

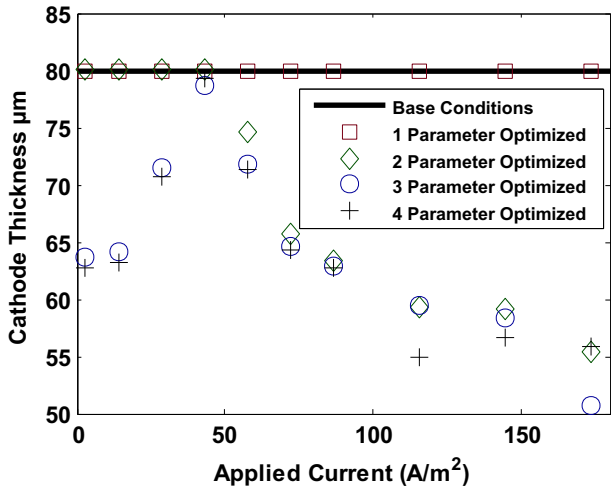

Fig. 8. Variation of the optimal cathode thickness (l_p) with applied current for all of the optimizations.

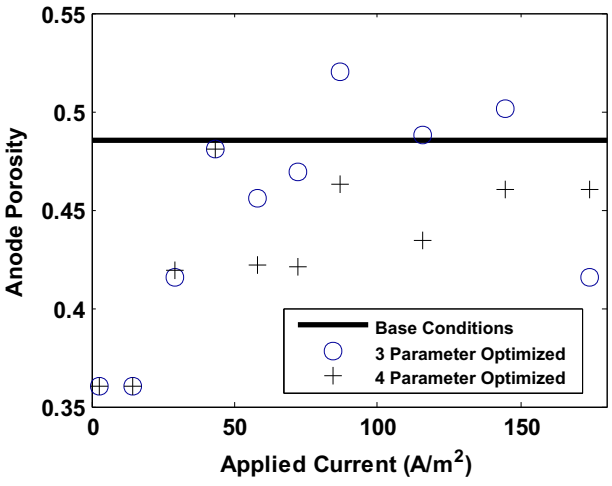

Fig. 10. Variation of the optimal anode porosity (ε_n) with applied current for the 3- and 4-parameter optimization.

the negligible improvement of specific energy for this optimization protocol from the base parameter case. For the 2-parameter optimization case, the cathode thickness does not vary considerably from the base values at low current densities, but for higher current densities the optimized values decrease from the base value. The cathode porosity variation for 2-parameter optimization shows that for low current densities the optimized values do not deviate considerably from the base values. For the lowest current density value it starts at a higher magnitude compared to the base value and decreases until it becomes almost equal to it for $i_{app} = 43.48125$ A m^{-2}. After that they increase from the base value as the current density increases. Therefore, the improvement in specific energy obtained is considerable for higher current densities as the optimized parameters obtained from the two-parameter optimization facilitate enhanced transport and kinetic behavior. For the 3-parameter optimization case, the optimized values for cathode thickness is less than the base values at low current densities but it increases and at $i_{app} = 43.48125$ A m^{-2} it becomes almost equal to the base parameter value. After that it again decreases considerably from the base value. The optimized cathode porosity variation for the three-parameter optimization follows a similar trend. It nearly hits the lower bound for low current densities but then climbs gradually as it approaches the base value at similar value of i_{app} mentioned previously. With the increase in current density the optimized cathode porosities continue to increase beyond the base value. It is observed that, at high current densities, the optimized cathode porosity and thickness do not vary much from the 2-parameter optimization case to the 3-parameter optimization protocol. This causes the negligible improvement observed in the specific energy for high i_{app} values between the two protocols. The variation in optimized anode porosity with current density approaches the lower bound at low applied current densities but increases at higher current densities but does not appear to follow any particular trend. It should be noted that the anode porosity was optimized along with the cathode parameters and the cell is cathode-limited. For increasing specific energy, lower values of electrode thickness and porosity look to be more desirable but the parameters are optimized in such a fashion that the strict minimum discharge time constraint is satisfied all times to give physically and practically meaningful optimized design parameters. This probably justifies the irregular variation of some of the optimized parameters.

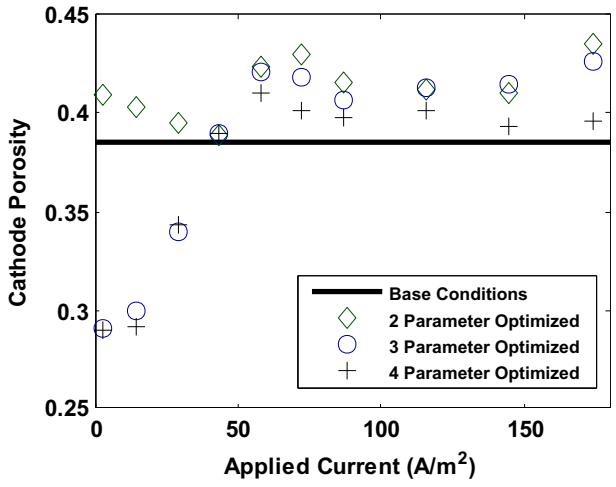

Fig. 9. Variation of the optimal cathode porosity (ε_p) with applied current for the 2-, 3-, and 4-parameter optimizations.

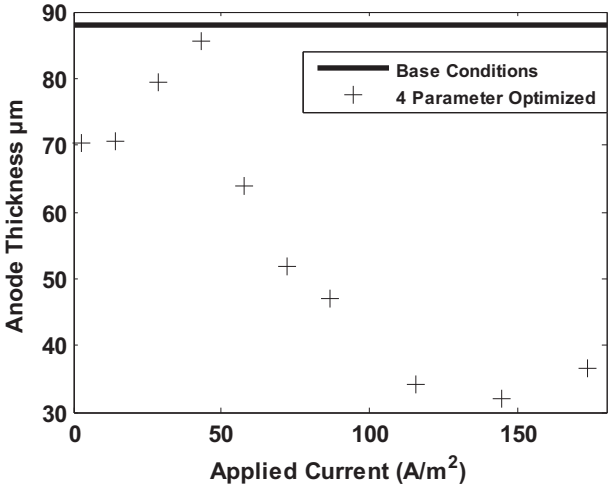

Fig. 11. Variation of the optimal anode thickness (l_n) with applied current for the 4-parameter optimization.

For four parameter optimization case, the variation of the optimized cathode thickness shows a trend similar to the 3-parameter optimization protocol. The optimized cathode porosity variation for 4-parameter optimization is again of similar trend as seen for the 3-parameter optimization case. For lower values of current densities, both 3- and 4-parameter optimization cases predict somewhat similar values for optimized cathode porosities but at higher currents slightly lower values are predicted which are very close to the base value. The optimized anode porosity profile shows similar irregular trends as the 3-parameter optimization case especially for the higher current densities. But for most current values, the optimized anode porosity gives lower values compared to those shown for 3-parameter optimization case except for $i_{app} = 173.925$ A m^{-2}. The optimized anode thickness profile is only available for the four parameter optimization case. As mentioned earlier, the criterion for electrode thickness ratio was not maintained for this protocol. For all values of applied current, the optimized anode thickness values are below the base parameter values. For other cases of optimization, the electrode thickness ratio criterion maintained the anode thickness to be greater than the cathode thickness. It should be kept in mind that the optimized parameter values for the 4-parameter optimization case, do not make any practical sense as the anode thickness was optimized simultaneously with the other variables without considering cost or possible discrepancies like unbalance of capacity on positive and negative sides of the sandwich etc. which are accounted for when using the electrode thickness constraint used in the other optimization schemes. These results are just for demonstration purposes and although they show increase in specific energy they should not be considered for design purposes.

3.8. Optimality of optimized parameters

There is a need to verify that the optimized electrode design parameters obtained are indeed optimal i.e. maximum specific energy is obtained when the electrode architecture is designed accordingly. To perform this check, the reformulated battery model was run with values of one of the optimized parameters ranging from lower bound to upper bound while the others were held at optimal conditions or at base conditions. From each simulation, the maximized specific energy obtained was plotted against the varied design parameter for all performed protocols of optimization. For example, optimized cathode thickness was plotted on the x-axis and maximized energy density on the y-axis, with cathode and anode porosities held at their optimal values for three-parameter optimization. Such plots will show the optimal solutions as peaks. The optimization protocols discussed in the paper follow a strict time constraint. The simulations for certain values of the optimized parameters did not satisfy this constraint and therefore the specific energy obtained has been set to zero for these cases. The $\times$ mark on the plots represents the optimal values of the varied selected parameter obtained from the optimization schemes.

Fig. 12 shows the plots of maximized energy density with variable cathode thickness for the different protocols of optimization at 2 C discharge rate. As expected, the optimal solutions are at the peaks of the plots. Another interesting observation is that after the optimal peak with decreasing magnitude of cathode thickness, the specific energy continues to decrease. This is the effect of thicker electrodes. Fig. 13 shows similar plots for varying cathode porosity at a 2 C discharge rate. For all the plots, the optimal values represent the peaks of the profiles. This trend verifies that the optimization protocols indeed give optimal values of design parameters for which the corresponding values of drawn specific energy are maxima. This also shows that the time constraint imposed on the optimization scheme largely determines the optimized values.

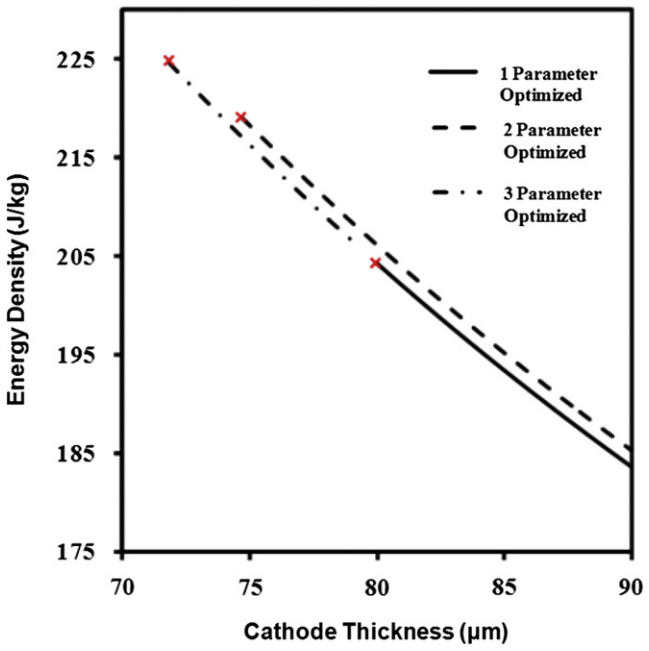

Fig. 12. Plot of the energy density drawn from the battery vs. varying cathode thickness (l_p). The red cross marks denote the optimal thickness for specific optimization protocol. (For interpretation of the references to color in this figure legend, the reader is referred to the web version of this article.)

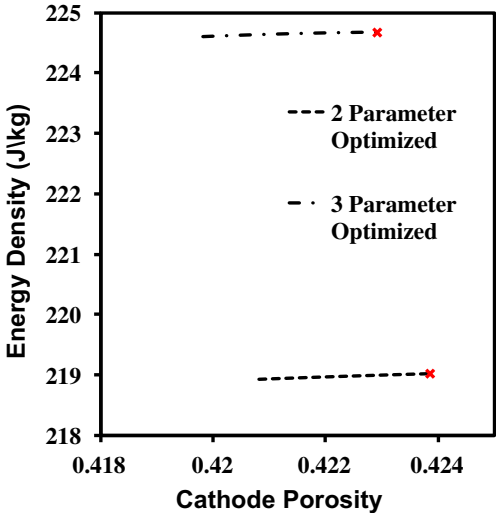

Fig. 13. Plot of the energy density drawn from the battery vs. varying cathode porosity (ε_p). The red cross marks denote the optimal porosity for specific optimization protocol. (For interpretation of the references to color in this figure legend, the reader is referred to the web version of this article.)

4. Conclusion

Simultaneous multi-parameter optimization of battery design parameters using a physics-based porous electrode theory model has been implemented for the efficient design of porous electrodes that are commonly used in advanced secondary batteries. Use of an orthogonal collocation-based reformulated model with increased computational efficiency facilitated the implementation. The results indicate that the simultaneous optimization of electrode

design parameters can result in a significant improvement in energy drawn from a battery. This study can be extended to the optimal design of state-of-the-art batteries for minimizing the temperature gradient across a cell for safe operation and prevention of thermal runaway. The adopted approach has applications in better design of batteries that can meet energy and power requirements for emerging applications in vehicles, satellites, and in the military. This procedure can also be extended to optimize other objectives such as maximizing the available discharge capacity given size constraints, rather than time constraints.

The analysis is based on a pseudo-2D macro-homogeneous model. Recent advances in the literature include multiscale models. Optimization based on those models will give results that will increase the utility of the proposed approach. However, note that as of today, dependency on having a fit for open circuit potential limits the applications of these new multiscale models.

Acknowledgments

This work was supported by the National Science Foundation under contract numbers CBET-0828002, and CBET-1008692; the International Center for Advanced Renewable Energy and Sustainability at Washington University in St. Louis (ICARES); and the U.S. government.

References

[1] M. Doyle, T.F. Fuller, J. Newman, J. Electrochem. Soc 140 (1993) 1526.
[2] C.M. Doyle, PhD dissertation, Dept. Chem. Eng., Univ. of California, Berkeley, CA, 1995.
[3] V. Srinivasan, J. Newman, J. Electrochem. Soc. 151 (2004) A1530.
[4] J. Christensen, V. Srinivasan, J. Newman, J. Electrochem. Soc. 153 (2006) A560.
[5] S. Stewart, P. Albertus, V. Srinivasan, I. Plitz, N. Pereira, G. Amatucci, J. Newman, J. Electrochem. Soc. 155 (2008) A253.
[6] T.F. Fuller, M. Doyle, J. Newman, J. Electrochem. Soc. 141 (1994) 982.
[7] T.F. Fuller, M. Doyle, J. Newman, J. Electrochem. Soc. 141 (1994) 1.
[8] M. Doyle, J. Newman, A.S. Gozdz, C.N. Schmutz, J.M. Tarascon, J. Electrochem. Soc. 143 (1996) 1890.
[9] K.E. Thomas, J. Newman, J. Electrochem. Soc. 150 (2003) A176.
[10] P. Arora, M. Doyle, A.S. Gozdz, R.E. White, J. Newman, J. Power Sources 88 (2000) 219.
[11] P. Ramadass, B. Haran, R.E. White, B.N. Popov, J. Power Sources 123 (2003) 230.
[12] P. Ramadass, B. Haran, P.M. Gomadam, R.E. White, B.N. Popov, J. Electrochem. Soc. 151 (2004) A196.
[13] G. Ning, R.E. White, B.N. Popov, Electrochim. Acta 51 (2006) 2012.
[14] G.G. Botte, V.R. Subramanian, R.E. White, Electrochim. Acta 45 (2000) 2595.
[15] P.M. Gomadam, J.W. Weidner, R.A. Dougal, R.E. White, J. Power Sources 110 (2002) 267.
[16] S. Santhanagopalan, Q. Guo, P. Ramadass, R.E. White, J. Power Sources 156 (2006) 620.
[17] V. Ramadesigan, P.W.C. Northrop, S. De, S. Santhanagopalan, R.D. Braatz, V.R. Subramanian, J. Electrochem. Soc. 159 (2012) R31–R45.
[18] J. Newman, W. Tiedemann, AIChE J. 21 (1975) 25.
[19] G.L. Plett, J. Power Sources 134 (2004) 252.
[20] L. Cai, R.E. White, J. Electrochem. Soc. 156 (2009) A154.
[21] V.R. Subramanian, V. Boovaragavan, V. Ramadesigan, M. Arabandi, J. Electrochem. Soc. 156 (2009) A260.
[22] P.W.C. Northrop, V. Ramadesigan, S. De, V.R. Subramanian, J. Electrochem. Soc. 158 (2011) A1461.
[23] J.C. Forman, S. Bashash, J.L. Stein, H.K. Fathy, J. Electrochem. Soc. 158 (2011) A93.
[24] J. Newman, J. Electrochem. Soc. 142 (1995) 97.
[25] V. Ramadesigan, R.N. Methekar, F. Latinwo, R.D. Braatz, V.R. Subramanian, J. Electrochem. Soc. 157 (2010) A1328.
[26] S. Golmon, K. Maute, M.L. Dunn, Meet. Abstr. Electrochem. Soc. 1101 (2011) 513.
[27] W. Du, A. Gupta, X. Zhang, A.M. Sastry, W. Shyy, Meet. Abstr. Electrochem. Soc. 1101 (2011) 1623.
[28] S. Kameswaran, L.T. Biegler, Comput. Chem. Eng. 30 (2006) 1560.
[29] A. Mitsos, B. Chachuat, P.I. Barton, J. Glob. Optim. 45 (2009) 63.
[30] R.N. Methekar, V. Ramadesigan, J.C. Pirkle, V.R. Subramanian, Comput. Chem. Eng. 35 (2011) 2227.

Nomenclature

E: specific energy density of the cell (W h kg^{-1})
V: potential drop across the cell (V)
i_{app}: applied current density (A m^{-2})
t: time (s)
M: mass per unit area (kg m^{-2})
ρ_n: density of negative electrode (kg m^{-3})
l_n: thickness of negative electrode (m)
ρ_p: density of positive electrode (kg m^{-3})
l_p: thickness of positive electrode (m)
ε_n: porosity of negative electrode
ε_p: porosity of positive electrode
$\varepsilon_{f,n}$: volume fraction of filler in negative electrode
$\varepsilon_{f,p}$: volume fraction of filler in positive electrode
ρ_e: density of electrolyte (kg m^{-3})
l_s: thickness of separator (m)
t_{d0}: total discharge time obtained by model simulation with base parameters (s)
t_d: total discharge time obtained by model simulation with optimized parameters (s)